Automated Determination of Martian Dust Devil Tracks Main Direction

Thiago Statella[1], Pedro Pina[2], Erivaldo Antônio da Silva[3]

[1] IFMT – Instituto Federal de Educação, Ciência e Tecnologia de Mato Grosso – Brasil
[2] CERENA - Centro de Recursos Naturais e Ambiente, Instituto Superior Técnico, Lisboa – Portugal
[3] UNESP – Universidade Estadual Paulista - Brasil

Dust Devils and their Tracks

Dust devils are vortices caused by unstable wind convection processes near the planetary surfaces, due to solar heat. An important information that can be obtained by the analysis of tracks produced by dust devils is the main direction taken by the vortices, which can be used to infer the main direction of the winds near the surface. Analyzing the main wind direction using digital images is useful, for example, to verify and improve predictions of the General Circulation Model (GCM). We then present and evaluate three automatic methods for calculating the main direction of tracks which have been detected previously by the method proposed by [1].

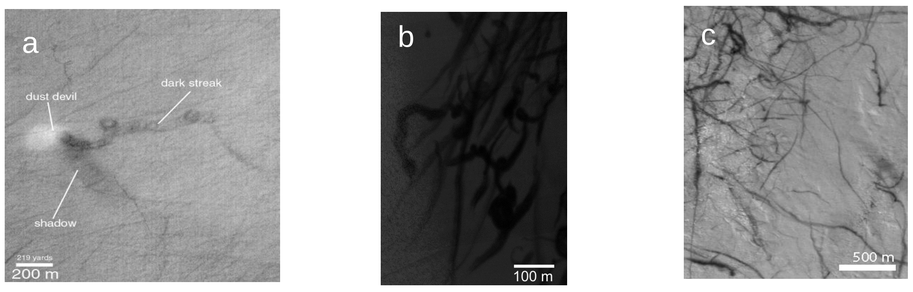

Fig. 1: Dust Devils and their tracks: (a) Dust devil on *Promethei Terra,* Mars (NASA/JPL/MSSS); (b) Dust devil tracks in the HiRISE image PSP-002548-1255 (NASA/JPL/University of Arizona); (c) Dust devil tracks in the MOC image E13-00271 (NASA/JPL/MSSS).

Methods

Method I: Gradient direction

This method uses the binary images with the tracks detected as input. The gradient direction $\alpha(x,y)$ was calculated by: $\alpha(x,y) = tg^{-1}(g_y / g_x)$ where g_y and g_x are Prewitt operators for first derivatives in y and x directions. The 4 main directions to be concerned are 0° (E-W), 45° (NE-SW), 90° (N-S) and 135° (NW-SE). The operation results in real values in the range [-180, 180] so negative angles were transformed in positives by subtracting them from 180°. After that, the real values in the range [0°, 180°] were classified to 0°-180°, 45°-225°, 90°-270° or 135°-315°. In this method, the main direction is given by the higher frequency among all four directions.

Method II: Directional morphological openings by Linear Structuring Elements (LSEs)

This method uses binary images with tracks detected as input. The morphological opening γ of f by a LSE B is the erosion ε of f by B followed by a dilation δ by B transposed [2]: $\gamma_B(f) = \delta_{\check{B}}(\varepsilon_B(f))$ with B being defined here as a function of size λ and direction α (each of the four main directions we were concerned). Size λ varied from scene to scene (though, for each scene, the size was fixed) according to the maximum width of the tracks in each scene. Tracks width was calculated as described in [1]. The main direction of the tracks is assumed to be the one in which the opening removed less pixels than the other directions.

Method III: Morphological granulometric analysis by Linear Structuring Elements

This method is similar to method II but differs in two aspects: 1) it uses the skeleton of the tracks as input data; and 2) the size of the SEs increases as each opening is carried out. The skeletonization was performed by the method proposed by [3]. For the granulometry we used a family $\Gamma = (\gamma_\lambda)_{\lambda \geq 0}$ of openings by scales $\lambda B = \{\lambda b \mid b \in B\}$, $\lambda \geq 0$, $\lambda \in Z$, B being a LSE. After applying those SEs, the main direction is defined as the one in which the accumulated frequency of removed pixels in a certain direction was higher, that is, we apply the granulometry in one direction and keep the sum of all pixels removed for each size of SE. Then we proceed the same way for the other 3 directions and compare the amount of pixels removed in each granulometry.

Results

The methods described were applied to a set of 190 MOC and HiRISE images (from regions Aeolis, Noachis, Argyre, Eridania and Hellas) containing tracks detected with an accuracy of ~92% ± 5%. The main direction obtained from each method and for each scene was compared to a ground truth set of directions defined visually by an expert. As an example, the main directions visually inferred for images MOC 12-02214 (Fig. 2(a)) and HiRISE ESP_013991_1160 (Fig. 2(b)) are, respectively, 90º-270° and 135º-315°.

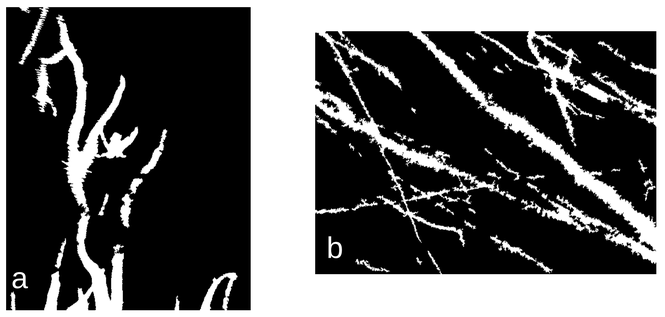

Fig. 2: Images MOC 12-02214 (a) and HiRISE ESP_013991_1160 (b) showing detected tracks.

The accuracy of the methods can be asserted by analysing the confusion matrix that is obtained by confronting, for each image, the main direction obtained by the automated method and the main direction visually defined by the expert. The global accuracy can then be calculated from the confusion matrix: $Accuracy = \sum x_{ii} / N$. Where x_{ii} are the elements of the main diagonal of the matrix and N is the total amount of observations. The accuracy of the method I was then 20.0%, that is, only 38 directions calculated by using the gradient agreed to the directions in the ground truth set defined visually. The accuracy for method II was 86.3% and for method III it was 66.3%. Table 1 shows directions inferred for images presented in Fig. 1 calculated using the three methods and the directions defined visually.

Table 1: Directions calculated using the three methods discussed and inferred visually for images MOC 12-02214 and HiRISE ESP_013991_1160.

	MOC	HiRISE
Method I	45°-225°	135°-315°
Method II	90°-270°	135°-315°
Method III	90°-270°	45°-225°
Visual	90°-270°	135°-315°

The low accuracy of method III is due to the skeleton of the objects. If tracks were features of little or no variation in their edges, the skeleton would represent the object direction more accurately. However, variations in the edge of tracks produce skeleton segments whose directions differ greatly from the direction of the main components to which they belong. The same variations in edges were responsible for the low accuracy of method I, specially for HiRISE, because of their higher resolution. The gradient directions were calculated for each pixel in the edge of tracks. As these edges are extremely irregular, showing a number of pixels oriented in directions other than the main one, the method failed in many cases. In the case of image MOC 12-02214 the mistake in the direction estimated by method I was probably caused in the step of classification of the directions in the interval [0°, 180°] to the classes 0°-180°, 45°-225°, 90°-270° and 135°-315°. Additional validation of the results obtained by our approach can also be performed, by confronting the main directions of the tracks with those predicted by the GCM. The main tracks directions for Argyre region were calculated using method II and compared to the directions predicted by the GCM. Table 2 shows the results. All directions inferred by method II agreed with those predicted by the GCM. The main direction of the wind in the region of Argyre in the solar longitudes ranging from 240° to 360° was E-W.

Table 2: Directions predicted by GCM and calculated using Method II for Argyre region.

Ls(°)	Images	Predicted	Inferred
240°-270°	7	E-W	E-W
270°-300°	7	E-W	E-W
300°-330°	15	E-W	E-W
330°-360°	42	E-W	E-W

Conclusions

A set of 190 MOC and HiRISE images with tracks detected previouslly was processed and the directions obtained were compared with a set of ground truth directions inferred viasually. Method I and III showed lower accuracies (20% and 66%, respectivelly) and Method II was the best one. From the tracks detected with an accuracy of ~92% ± 5%, the directional openings by LSEs could infer the main direction of tracks with an accuracy of ~86%. Besides, when comparing the directions inferred for Argyre region to those predicted by the GCM the results agree. In such case, the wind direction predicted and inferred was E-W. Therefore, method II can be used to infer automatically and accurately the direction of winds from Martian dust devil tracks.

References

[1] Statella et al. (2012) *PSS*, 70, 46-58. [2] Soille P. (2004), *Morphological Image analysis*. [3] Zhang T. Y. and Suen C. Y. (1984) *Communications of the ACM*, 27, 236-239.